

# TWO-PHOTON EXCITATION OF QUANTUM DOT DONORS IN FLUORESCENCE RESONANCE ENERGY TRANSFER APPLICATIONS

Aaron R. Clapp<sup>1</sup>, Thomas Pons<sup>2</sup>, Igor L. Medintz<sup>2</sup>, James B. Delehanty<sup>2</sup>, Philip E. Dawson<sup>3</sup>, and Hedi Mattoussi<sup>2</sup>

<sup>1</sup>Iowa State University, Ames, IA

<sup>2</sup>Naval Research Laboratory, Washington, DC

<sup>3</sup>The Scripps Research Institute, La Jolla, CA

## Introduction

Luminescent quantum dots (QDs), having large absorption cross-sections, excellent photostability, broad excitation and narrow emission spectra, are attractive and increasingly popular alternatives to organic dyes for fluorescence labeling and emerging nanosensing applications [1-10]. Through chemical modification of the nanocrystal surface ligands (including complete ligand exchange and encapsulation methods), QDs can be stably dispersed in aqueous solutions [3-5,10]. This has led to their use in biological investigations, most notably in cellular labeling [3,4,6,7,10], and in the development of fluorescence assays that can detect small molecules and oligonucleotides in solution [8,9]. Several groups have shown that QDs are efficient donor fluorophores for fluorescence resonance energy transfer (FRET) where multiple acceptor dyes can be positioned around the QD to significantly enhance the FRET efficiency between QDs and nearby dyes [11-18]. Because of its sensitivity to changes in donor-acceptor separation distance (varying with the sixth power), FRET has proved to be a useful method for detecting molecular scale interactions, such as binding events and changes in protein conformations. FRET-based QD-protein and QD-peptide sensing assemblies that are specific for the detection of target molecules including soluble TNT and the activity of various proteolytic enzymes have been demonstrated [14,19,20].

Multi-photon fluorescence microscopy is a popular imaging method for relatively thick (~1 mm) tissue samples due to its small focal volume and limited out-of-focus photodamage. It also uses far red and near infrared excitation which is ideally located in the tissue optical transparency window [21]. However, FRET performance driven by two-photon excitation has been limited by the photophysical properties of organic dyes and fluorescent proteins. In particular, it is difficult to implement a donor-acceptor pair with substantial spectral overlap for high FRET efficiency and non-overlapping two-photon absorption spectra for limited acceptor direct excitation. Larson *et al.* showed that water-soluble CdSe-ZnS QDs are superior probes for multi-photon fluorescence imaging where typical QD two-photon action cross-sections are about one to two orders of magnitude larger than those of organic molecules designed specifically for such applications [22].

We demonstrate resonance energy transfer between luminescent QDs and nearby dye acceptors initiated by a two-photon excitation process. Energy transfer between QDs and localized organic dyes has two unique features in this format. First, it exploits the very high two-photon action cross-sections of QDs compared to those of conventional dyes, which results in a nearly undetectable background contribution from the dye acceptors due to direct excitation. Second, it provides high signal-to-background ratios in FRET imaging of cells and tissues by effectively eliminating autofluorescence and direct excitation contributions to the

acceptor photoluminescence (PL) signal. These features can considerably improve subsequent data interpretation when signals of both QD donor and dye acceptor are required to quantify the results. They can also improve applications such as intracellular sensing where FRET interactions are used to report events within the cell. We also show that the energy transfer resulting from two-photon excitation is consistent with results using one-photon excitation, and in agreement with predictions of Förster theory.

## Materials and Methods

### ***Quantum dot-protein conjugates***

*E. coli* maltose binding protein was engineered with C-terminal polyhistidine (MBP-His) to induce metal affinity self-assembly on the surface of DHLA-functionalized QDs [13,14]. These proteins were also modified to contain cysteine point mutations (at positions D41C or D95C) for specific labeling with maleimide-functionalized Cy3 dye prior to conjugate assembly. MBP-His labeled at D95C was used for the steady state and time-resolved fluorescence experiments, while MBP-His labeled at D41C was exclusively used in the reagentless sensor design. The overall MBP-to-QD ratio was maintained at 15:1 which saturated the QD surface and maintained a consistent QD quantum yield due to surface passivation [13].

### ***Quantum dot-peptide conjugates***

Cell-penetrating peptide (CPP) was synthesized using standard solid phase peptide synthesis with the sequence (His)<sub>8</sub>-Trp-Gly-Leu-Ala-Aib-Ser-Gly-(Arg)<sub>8</sub>-amide, where Aib is the artificial residue alpha-amino isobutyric acid. The Cy3-labeled peptide was synthesized with the sequence, Ac-(His)<sub>6</sub>-Gly-Leu-Aib-Ala-Ala-Gly-Gly-His-Tyr-Gly-Cys-NH<sub>2</sub>, where Ac is an acetyl group at the N-terminus. This peptide was labeled with a maleimide-functionalized Cy3 (Amersham Biosciences, Piscataway, NJ) at the cysteine residue. The polyhistidine sequences at the N-termini of the peptides directed their self-assembly on the QD surface. QD conjugate stock solutions were prepared by incubating 1  $\mu$ M of DHLA-capped QDs with the appropriate ratios of peptides, i.e., 60 CPP per QD for CPP-QD conjugates, or 60 CPP mixed with 2 peptide-Cy3 per QD for CPP-QD-peptide-Cy3 mixed-surface conjugates.

### ***Two-photon excited steady-state spectra***

Two-photon excitation was generated using a tunable Ti:sapphire laser (200 fs pulse width, 76 MHz, Clark-MXR, Dexter, MI) operating at 800 nm and focused with an objective lens to a diffraction-limited spot within a quartz cuvette containing the bioconjugate sample. Fluorescence spectra were collected using a spectrometer (SPEX 270M, HORIBA Jobin Yvon, Edison, NJ).

### ***Fluorescence lifetimes***

The excitation source for the time-resolved experiments used the pulse-picked output (5 MHz) of a mode locked Ti:sapphire oscillator (pulse width <200 fs, Mira 900, Coherent, Santa Clara, CA) with a center wavelength at 800 nm. Photoluminescence was detected using an avalanche photodiode (APD, SPCM-AQR-13, PerkinElmer, Wellesley, MA), and lifetimes were determined using a time correlated single photon counting (TCSPC) system equipped with a TimeHarp 200 card and software (PicoQuant GmbH, Berlin, Germany).

## **Cell imaging**

Two-photon cell imaging was performed with a Bio-Rad MRC-1024MP confocal system (Bio-Rad, Hercules, CA) using ~10 mW of 840 nm pulsed excitation (~80 fs, 80 MHz, Tsunami, Spectra-Physics, Mountain View, CA) at the focal plane of a 60×, 0.9 NA water immersion objective (E600FN upright microscope, Nikon, Melville, NY). DAPI, 510 nm QD, and Cy3 signals were separated using 490 nm and 550 nm dichroics. DAPI fluorescence cross-talk was subtracted from the QD channel. One-photon cell imaging of the same samples was performed with an Olympus IX71 inverted microscope and a Princeton Instruments I-PentaMAX CCD camera (Photometrics, Tucson, AZ). DAPI fluorescence was imaged using 350 nm excitation from a Xe lamp, while QDs and Cy3 were excited with a 488 nm Ar ion laser and spectrally separated using a 565 nm dichroic mirror.

## **Results and Discussion**

### **Two-photon action cross-sections**

Table 1 shows the two-photon action cross-section values measured for our QDs in toluene and water solutions, along with those of traditional dyes for comparison.

**Table 1.** Two photon action cross-sections

sample	Two-photon action cross-section (GM, 800 nm)	
	water	toluene
510 nm QDs	8500	-
540 nm QDs	13800	15000
555 nm QDs	23200	19500
570 nm QDs	-	23000
Cy3	<1	-
Fluorescein	36	-
GFP	6	-

Measured values for QDs are at least two orders of magnitude higher than Cy3 or those reported in the literature for other common organic dyes [23,24]. These values are consistent with previously reported two-photon action cross-sections for CdSe-ZnS QDs.

### **Steady-state PL measurements**

Steady-state composite spectra from samples excited by two-photon excitation were deconvoluted to yield individual PL contributions using the previously-recorded spectral profiles of individual QD samples and Cy3 dye emission (see Figure 1). In all cases, the PL contribution due to direct excitation was measured using control samples containing MBP-Cy3 alone and subtracted from the composite spectra before analysis. The QD PL spectra collected using a two-photon excitation mode maintain the same symmetric and narrow features as those collected in the one-photon excitation mode.

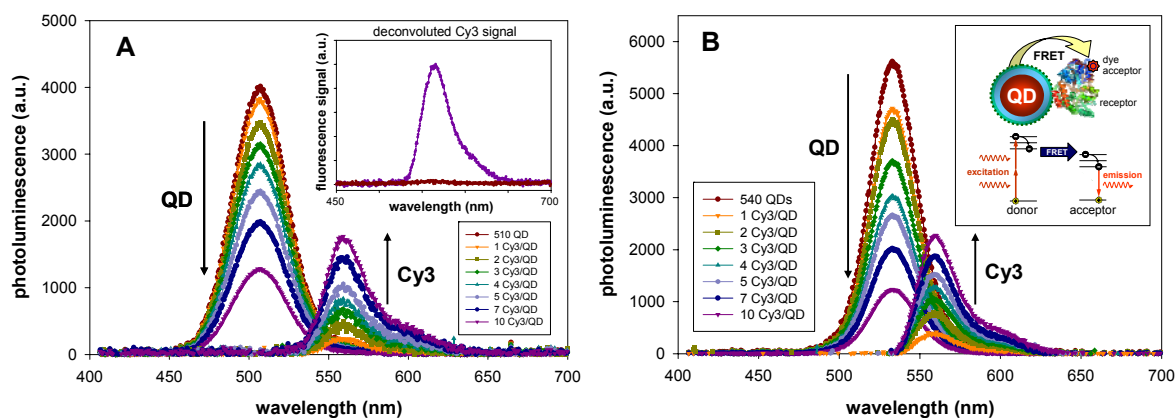


**Figure 1.** PL spectra of QDs and localized Cy3 as a function of the number of MBP-Cy3 per QD using two-photon excitation: (A) 510 nm QDs (inset: direct versus FRET-induced excitation of Cy3) and (B) and 540 nm QDs (inset: schematic of two-photon excitation process).

### Time-resolved PL measurements

Time-resolved fluorescence measurements show a pronounced decrease in QD donor lifetime for solutions of QD-MBP-Cy3 compared with bare nanocrystals (see Figure 2). The data also show that the Cy3 lifetime increases in the QD conjugate as compared to Cy3 alone. This observation is consistent with results using a one-photon excitation mode [13,14]. A decrease in QD steady-state PL and radiative lifetime were negligible when QDs were mixed with free dye (control samples) due to negligible FRET interactions.

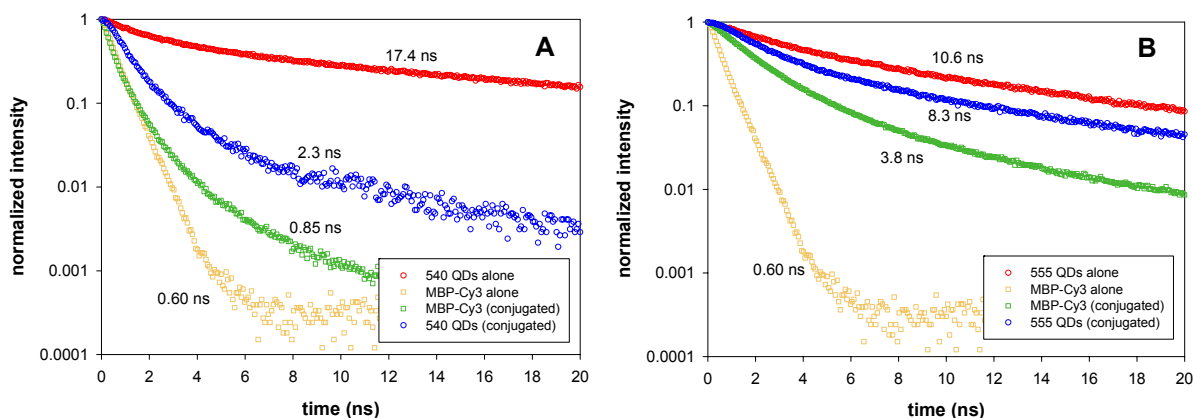


**Figure 2.** Time-resolved fluorescence decays for (A) 540 nm QD-MBP-Cy3 and (B) 555 nm QD-MBP-Cy3 where PL signals from donor and acceptor are spectrally isolated by appropriate band pass filters. Decay profiles are shown for isolated QDs, isolated MBP-Cy3, and for each fluorophore when co-localized in a conjugate.

### Quantitative analysis of titration data

The results above indicate that the loss of QD emission is specifically due to self-assembly of the dye-labeled protein on the nanocrystal surface, which positions the dye acceptors close to the QD donor. This leads to efficient non-radiative transfer of excitation energy from the QD to the proximal Cy3 dye. The experimental ensemble FRET efficiency can be readily determined using the relation (developed for one-photon excitation FRET):

$$E = 1 - \frac{F_{DA}}{F_D}, \quad (1)$$

where  $F_{DA}$  and  $F_D$  are the QD PL measured in the presence and absence of dye acceptors, respectively [25]. Figure 1 shows that the FRET efficiency increases with the number of dyes positioned near the QD surface,  $n$ . The data also show that the dependence of the FRET efficiency on the ratio  $n$  for the two-photon excitation mode is indistinguishable from the results using one-photon excitation. The improved FRET efficiency with an increasing number of dyes is due to the increased effective overlap integral when multiple acceptors interact with a central QD donor [13,14,25]. However, the two-photon excitation mode effectively eliminated undesired direct excitation PL contribution common to one-photon excitation of these conjugates. This improvement is due to a markedly smaller two-photon absorption cross-section (by a factor of  $\sim 10^4$ ) for the dye relative to QDs, indicating that the entire Cy3 signal from the QD-dye conjugates is attributable to non-radiative energy transfer (see Figure 1A inset). This is a desirable advantage over a one-photon mode where direct excitation of the acceptor, though sometimes small for an optimized excitation wavelength, must be subtracted from the composite spectra to properly estimate the FRET efficiency. Analysis of the QD PL loss (or  $E$ ) using Förster's formalism provided estimates of average donor-acceptor distances  $r$  for both assemblies using the formula:

$$r = R_0 \left[ \frac{n(1-E)}{E} \right]^{1/6}, \quad (2)$$

where  $R_0$  is the Förster distance [13,25]. The 510 nm QD-MBP-Cy3 and 540 nm QD-MBP-Cy3 titration results yielded fitted distances of  $67 \pm 5$  and  $72 \pm 4$  Å, respectively, consistent with other measurements for these QD bioconjugates and with values extracted using one photon excitation mode [13]. The point dipole approximation assumed in Förster theory is thus considered to be sufficient for describing QD fluorophores in these systems [26].

### ***Intracellular imaging of FRET interactions***

We next demonstrate a unique advantage of two-photon excitation to study energy transfer between QDs and conjugated dye acceptors, while investigating the stability of self-assembled QD-peptide conjugates within cells using fluorescence microscopy. Long-term stability of QD-protein conjugates is a fundamental requirement in the design of QD-based intracellular sensors. 510 nm emitting QDs were conjugated with polyarginine-rich cell-penetrating peptides (CPP) containing N-terminal polyhistidine, and subsequently incubated with human embryonic kidney (HEK 293T/17) cells (at a ratio of  $\sim 60$  peptides per QD, 50 nM QD) for 1 hour and fixed [27]. These peptides are known to induce endocytosis of conjugated cargos such as proteins or nanoparticles in a variety of cell lines [28,29]. Two-photon excited fluorescence images of these cells displayed punctate QD staining indicative of endosomal uptake (Figure 3A), a feature that was absent when the cells were exposed to QDs alone. When QDs were conjugated to both CPP and Cy3-labeled peptides (CPP-QD-peptide-Cy3, with 2 Cy3 per QD), we observed efficient FRET from QDs to Cy3, as shown in Figure 3B. In contrast, staining the cells with a mixture of Cy3-labeled transferrin (Tf-Cy3), a common endosomal marker, and unlabeled CPP-QD does not show evidence of Cy3 PL (Figure 3C).

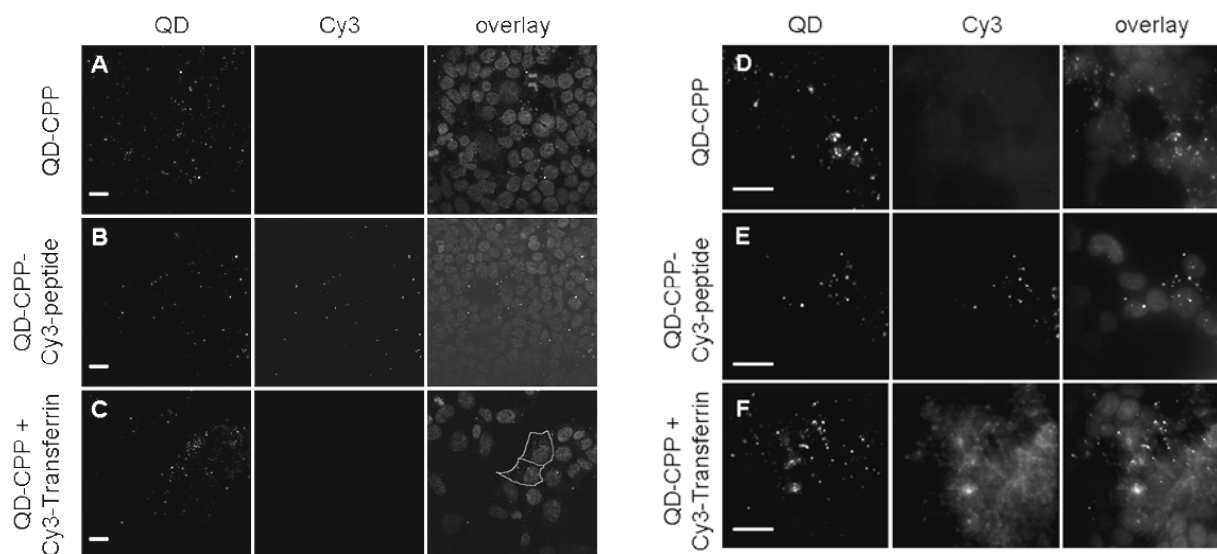


**Figure 3. (A-C)** Two-photon fluorescence images of cells following incubation with 510 nm QDs conjugated to: (A,C) CPP, (B) CPP and 2 Cy3-labeled peptide. In (C), the cells were also incubated with Cy3 labeled-transferrin (not bound to QDs). **(D-F)** One-photon fluorescence images cells corresponding to (A-C), respectively. (scale bar = 20  $\mu\text{m}$ .)

In the latter case, the dye was not directly conjugated to the QDs, which prevented efficient FRET interactions. We compared these two-photon fluorescence images with the corresponding one-photon epifluorescence images using 488 nm excitation (Figure 3D-F). While similar images were observed when cells were exposed to CPP-QD and CPP-QD-peptide-Cy3 conjugates, the cells showed bright Cy3 labeling upon exposure to a mixture of CPP-QD and Tf-Cy3 (compare Figure 3C and F). This demonstrates that significant Cy3 direct excitation occurred upon one-photon excitation at 488 nm (Figure 3F). As a consequence, it is impossible to distinguish between Cy3 emission due to FRET and direct excitation in a one-photon mode, without additional background correction and image processing. Conversely, PL signal due to direct excitation of the acceptor dye was not observed in a two-photon excitation mode even at 20-fold molar excess relative to the QD donor. The absence of direct excitation of the acceptor is a unique advantage of two-photon excited FRET using QD donors. Two-photon excitation unambiguously reveals co-localized fluorophores and efficient energy transfer from QDs to dyes when QD-peptide-dye conjugates are formed prior to endocytosis. This also demonstrates that the labeled peptides remained stably conjugated to QDs within the endosomal compartments after 72 hours.

### **Two-photon FRET sensing**

We combined the advantages of two-photon excitation and FRET to implement a reagentless sensor specific for the sugar maltose. In this arrangement, MBP-His was labeled at the unique D41C residue such that binding to maltose induces a conformational change, which alters the PL of Cy3 [30]. The FRET efficiency does not change as the maltose concentration increases, rather the PL of the acceptor varies with changes in Cy3 quantum yield. Figure 4A shows the steady-state conjugate PL with increasing maltose concentration.

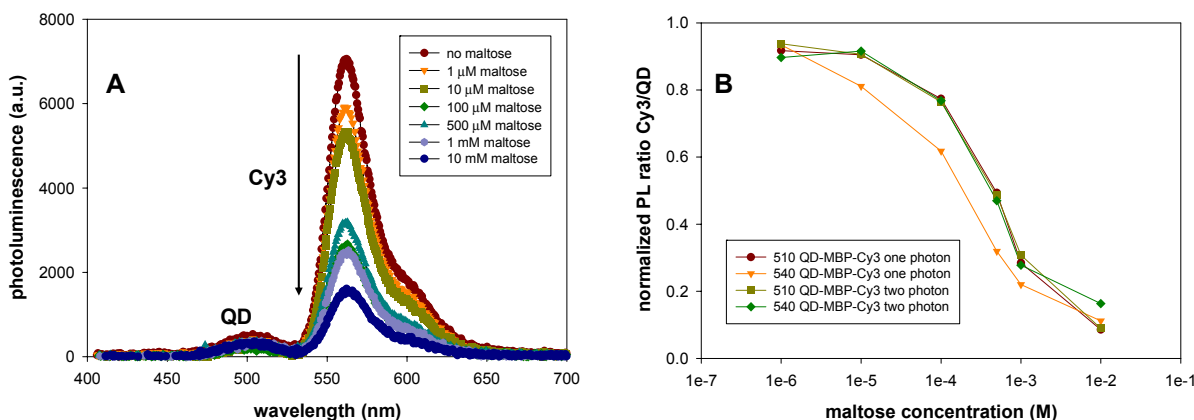


**Figure 4. (A)** Spectra from a reagentless sensing format using 510 nm QDs with MBP-Cy3. **(B)** Integrated PL versus maltose concentration for four arrangements using 510 nm and 540 nm QDs with MBP-Cy3 in one and two-photon excitation modes.

Figure 4B shows measured PL ratios as a function of maltose concentration using 510 and 540 nm emitting QDs in one and two-photon excitation modes. As the maltose concentration approaches the equilibrium dissociation constant,  $K_D$ , the Cy3 PL drops dramatically. A  $K_D$  of 0.8 mM was measured for this sensing assembly demonstrating that its response is consistent independent of the QD or excitation method used [30]. In a two-photon mode, the QD functions as a light-harvesting fluorophore where exciton energy is transferred from QD to dye.

## Conclusions

Multi-photon excitation of QDs offers several unique advantages for fluorescence imaging which extend to FRET-based applications. Due to the large two-photon action cross-sections of luminescent CdSe-ZnS QDs relative to dyes, direct excitation and spectral cross-talk can be significantly reduced. As a result, detection of molecular-scale rearrangements (e.g., binding, protein folding/denaturation, enzymatic cleavage) via FRET can be simplified and improved using two-photon excitation. As intracellular nanosensing evolves, multi-photon excitation will afford revealing images of structures and pathways. The interchangeable use of one and two-photon excitation modes in FRET-based sensing allows for the design and characterization of these tools prior to more complicated *in vivo* implementation. This generalized approach can be used to develop new sensing schemes for real-time intracellular detection, which are compatible with multi-photon imaging techniques.

## References

1. X. Michalet, F.F. Pinaud, L.A. Bentolila, J.M. Tsay, S. Doose, J.J. Li, G. Sundaresan, A.M. Wu, S.S. Gambhir, S. Weiss, *Science* **307**, 538-544 (2005).
2. I.L. Medintz, H.T. Uyeda, E.R. Goldman, and H. Mattoussi, *Nat. Mater.* **4**, 435-446 (2005).
3. M. Bruchez, M. Moronne, P. Gin, S. Weiss, A.P. Alivisatos, *Science* **281**, 2013-2015 (1998).

4. W. Chan and S. Nie, *Science* **281**, 2016-2018 (1998).
5. H. Mattoussi, J.M. Mauro, E.R. Goldman, G.P. Anderson, V.C. Sundar, F.V. Mikulec, M.G. Bawendi, *J. Am. Chem. Soc.* **122**, 12142-12150 (2000).
6. X. Wu, H. Liu, J. Liu, K.N. Haley, J.A. Treadway, J.P. Larson, N. Ge, F. Peale, M.P. Bruchez, *Nat. Biotech.* **21**, 41-46 (2003).
7. J.K. Jaiswal, H. Mattoussi, J.M. Mauro, S.M. Simon, *Nat. Biotech.* **21**, 47-51 (2003).
8. E.R. Goldman, G.P. Anderson, P.T. Tran, H. Mattoussi, P.T. Charles, J.M. Mauro, *Anal. Chem.* **74**, 841-847 (2002).
9. D. Gerion, W.J. Parak, S.C. Williams, D. Zanchet, C.M. Micheel, A.P. Alivisatos, *J. Am. Chem. Soc.* **124**, 7070-7074 (2002).
10. B. Dubertret, P. Skourides, D.J. Norris, V. Noireaux, A.H. Brivanlou, A. Libchaber, *Science* **298**, 1759-1762 (2002).
11. P.T. Tran, E.R. Goldman, G.P. Anderson, J.M. Mauro, and H. Mattoussi, *Phys. Stat. Sol. (b)* **229**, 427-432 (2002).
12. F. Patolsky, R. Gill, Y. Weizmann, T. Mokari, U. Banin, I. Willner, *J. Am. Chem. Soc.* **125**, 13918-13919 (2003).
13. A.R. Clapp, I.L. Medintz, J.M. Mauro, B.R. Fisher, M.G. Bawendi, H. Mattoussi, *J. Am. Chem. Soc.* **126**, 301-310 (2004).
14. I.L. Medintz, A.R. Clapp, H. Mattoussi, E.R. Goldman, J.M. Mauro, *Nat. Mater.* **2**, 630-638 (2003).
15. J.H. Kim, D. Morikis, M. Ozkan, *Sens. Actuators B* **102**, 315-319 (2004);
16. M. Levy, S.F. Cater, A.D. Ellington, *ChemBioChem.* **6**, 2163-2166 (2005)
17. C.Y. Zhang, H.C. Yeh, M.T. Kuroki, and T.H. Wang, *Nat. Mater.* **4**, 826-831 (2005).
18. H.E. Grecco, K.A. Lidke, R. Heintzmann, D.S. Lidke, C. Spagnuolo, O.E. Martinez, E.A. Jares-Erijman, T.M. Jovin, *Microscopy Res. Technique*, **65**, 169-179 (2004).
19. E.R. Goldman, I.L. Medintz, J.L. Whitley, A. Hayhurst, A.R. Clapp, H.T. Uyeda, J.R. Deschamps, M.E. Lassman, H. Mattoussi, *J. Am. Chem. Soc.* **127**, 6744-6751 (2005).
20. I.L. Medintz, A.R. Clapp, F.M. Brunel, T. Tiefenbrunn, H.T. Uyeda, E.L. Chang, J.R. Deschamps, P.E. Dawson, and H. Mattoussi, *Nat. Mater.* **5**, 581-589 (2006).
21. W. Denk, J.H. Strickler, W.W. Webb, *Science* **248**, 73-76 (1990).
22. D.R. Larson, W.R. Zipfel, R.M. Williams, S.W. Clark, M.P. Bruchez, F.W. Wise, W.W. Webb, *Science* **300**, 1434-1436 (2003).
23. M.A. Albota, C. Xu, W.W. Webb, *Appl. Opt.* **37**, 7352-7356 (1998).
24. C. Xu, W. Zipfel, J. B. Shear, R. M. Williams, and W. W. Webb, *Proc. Nat. Acad. Sci. U.S.A.* **93**, 10763-10768 (1996).
25. J.R. Lakowicz, *Principles of Fluorescence Spectroscopy*, 2nd Ed. (Kluwer Academic/Plenum Publishers, 1999).
26. A.R. Clapp, I.L. Medintz, and H. Mattoussi, *Chem. Phys. Chem.* **7**, 47-57 (2006).
27. J.B. Delehanty, I.L. Medintz, T.Pons, P.E. Dawson, F.M. Brunel, and H. Mattoussi, *Bioconjugate Chemistry* **17**, 920-927 (2006).
28. S. Fawell, J. Seery, Y. Daikh, C. Moore, L.L. Chen, B. Pepinsky, J. Barsoum, *Proc. Natl. Acad. Sci. U.S.A.* **91**, 664-668 (1994).
29. L. Josephson, C.H. Tung, A. Moore, R. Weissleder, *Bioconj. Chem.* **10**, 186-191 (1999).
30. I.L. Medintz, A.R. Clapp, J.S. Melinger, J.R. Deschamps, and H. Mattoussi, *Adv. Mater.* **17**, 2450-24